Available online at www.sciencedirect.com
SCIENCE DIRECT®
Physica A 364 (2006) 423–434
PHYSICA A
www.elsevier.com/locate/physa

Phase-rectified signal averaging detects quasi-periodicities in non-stationary data

Axel Bauer[a], Jan W. Kantelhardt[b,*], Armin Bunde[c], Petra Barthel[a], Raphael Schneider[a], Marek Malik[d], Georg Schmidt[a]

[a]*Medizinische Klinik und Deutsches Herzzentrum München der Technischen Universität München, Germany*
[b]*Fachbereich Physik und Zentrum für Computational Nanoscience, Martin-Luther-Universität, Halle (Saale), Germany*
[c]*Institut für Theoretische Physik III, Justus-Liebig-Universität, Giessen, Germany*
[d]*Department of Cardiac and Vascular Sciences, St. George's, University of London, UK*

Received 18 August 2005
Available online 18 October 2005

Abstract

We present an efficient technique for the study of quasi-periodic oscillations in noisy, non-stationary signals, which allows the assessment of system dynamics despite phase resetting and noise. It is based on the definition of anchor points in the signal (in the simplest case increases or decreases of the signal) which are used to align (i.e., phase-rectify) the oscillatory fluctuations followed by an averaging of the surroundings of the anchor points. We give theoretical arguments for the advantage of the technique, termed phase-rectified signal averaging (PRSA), over conventional spectral analysis and show in a numerical test using surrogate heartbeat data that the threshold intensity for the detection of additional quasi-periodic components is approximately 75% lower with PRSA. With the use of different anchor point criteria PRSA is capable of separately analysing quasi-periodicities that occur during increasing or decreasing parts of the signal. We point to a variety of applications in the analysis of medical, biological, and geophysical data containing quasi-periodicities besides non-stationarities and $1/f$ noise.

Keywords: Time-series analysis; Quasi-periodicities; Non-stationary behaviour; Synchronization; Long-term correlations

1. Introduction

In many natural signals periodicities occur on different time scales due to intrinsic closed-loop regulations within the controlling systems. In biology and physiology, e.g., cardiac rhythms, rhythmic motions of limbs in walking, muscle contractions, rhythms underlying the release of hormones that regulate growth and metabolism, periodicities in gene expression, membrane potential oscillations, oscillations in neuronal signals, and circadian rhythms are just a few of the many periodic phenomena (see, e.g., Refs. [1,2]). Oscillations also occur in geophysical data, e.g., for the El-Nino phenomenon, for sunspot numbers, and for ice age periods [3].

*Corresponding author. Tel.: +49 345 55 25433; fax: +49 345 55 25446.
E-mail address: kantelhardt@physik.uni-halle.de (J.W. Kantelhardt).

0378-4371/$ - see front matter © 2005 Elsevier B.V. All rights reserved.
doi:10.1016/j.physa.2005.08.080

Consequently, there are numerous applications where periodicities must be detected from experimental data [4]. Non-stationarities, however, are a major problem in the analysis of signals that are recorded from composite systems over a prolonged period of time. Many internal and external perturbations are continuously influencing the systems causing interruptions of the periodic behaviour. The interruptions often 'reset' the regulatory processes resulting in phase de-synchronization of the oscillations. The signal thus becomes *quasi-periodic*, consisting of many periodic patches, where the typical length of the patches defines the *coherence time* of the quasi-periodicity. Such signals cannot be comprehensively quantified by conventional methods, e.g., spectral analysis, that compare the signal with long sinusoids of different frequency without phase resets. Moreover, any measurement of a biological system is, as a rule, noise polluted, $1/f$ noise being particularly prevalent.

Here, we propose a novel signal processing technique, termed phase-rectified signal averaging (PRSA), which is capable of detecting and quantifying quasi-periodic oscillations masked by the non-stationary nature of composite signals and noise. The method also allows to quantify the typical coherence time for each quasi-periodicity and to separate processes occurring during increasing and decreasing parts of the signal.

The paper is organized as follows. In Section 2 we describe the method by giving the main idea as well as several variants that seem appropriate in some of the applications. Section 3 is devoted to the comparison of the PRSA method with conventional spectral analysis based on Fourier transform. In Section 4 we discuss parameters that can be derived from the phase-rectified signal average to characterize the quasi-periodicities in the signal. In Section 5 we describe the results of a numerical test we performed to study the capacity of the analysis technique, and discuss possible applications of the method.

2. Description of the PRSA technique

We consider a long time series (signal) (x_i), $i = 1, \ldots, N$, which in addition to relevant periodicities and correlations, may exhibit non-stationarities, artefacts, and noise.[1] One example for such a signal is the series of time intervals between successive heartbeats determined from a long-term ECG of a patient. Our aim is to compress the signal into a much shorter sequence, keeping all relevant quasi-periodicities but eliminating non-stationarities, artefacts, and noise.

The basic PRSA principle is the aligning of sections of the series relative to selected anchor points followed by a signal averaging, as we explain in the following. The method consists of three steps as illustrated in Fig. 1.

In the *first step* (see Fig. 1(a)), anchor points (i.e., some of the indices i) are selected according to certain properties of the signal (x_i). There are several possibilities: in the most simple version of the PRSA method, the anchor points correspond to increases in the signal (increase events),

$$x_i > x_{i-1} \tag{1a}$$

or to decreases in the signal (decrease events),

$$x_i < x_{i-1}. \tag{1b}$$

Alternatively, one may define the anchor points by comparing averages of T values of the time series,

$$\frac{1}{T}\sum_{j=0}^{T-1} x_{i+j} > \frac{1}{T}\sum_{j=1}^{T} x_{i-j} \tag{2a}$$

or

$$\frac{1}{T}\sum_{j=0}^{T-1} x_{i+j} < \frac{1}{T}\sum_{j=1}^{T} x_{i-j}. \tag{2b}$$

[1] If the original signal (x_i) is not homogeneously sampled in time, it might be necessary to apply a resampling procedure, where (x_i) is replaced by the resampled series $(\tilde{x}_i)$, $i = 1, \ldots, N'$ corresponding to interpolated measurements $\tilde{x}_i$ at times $t_i = i\Delta t$ with an appropriate time resolution Δt and $N'\Delta t$ the total duration of the recording. Such a resampling procedure is often applied, e.g., for heartbeat time interval series in order to obtain real frequencies in spectral analysis. The resampling procedure allows indices to be interpreted in terms of time scale. In series obtained under unreliable recording conditions, however, the resampling procedure might increase the number of artefacts and thus might be disadvantageous.

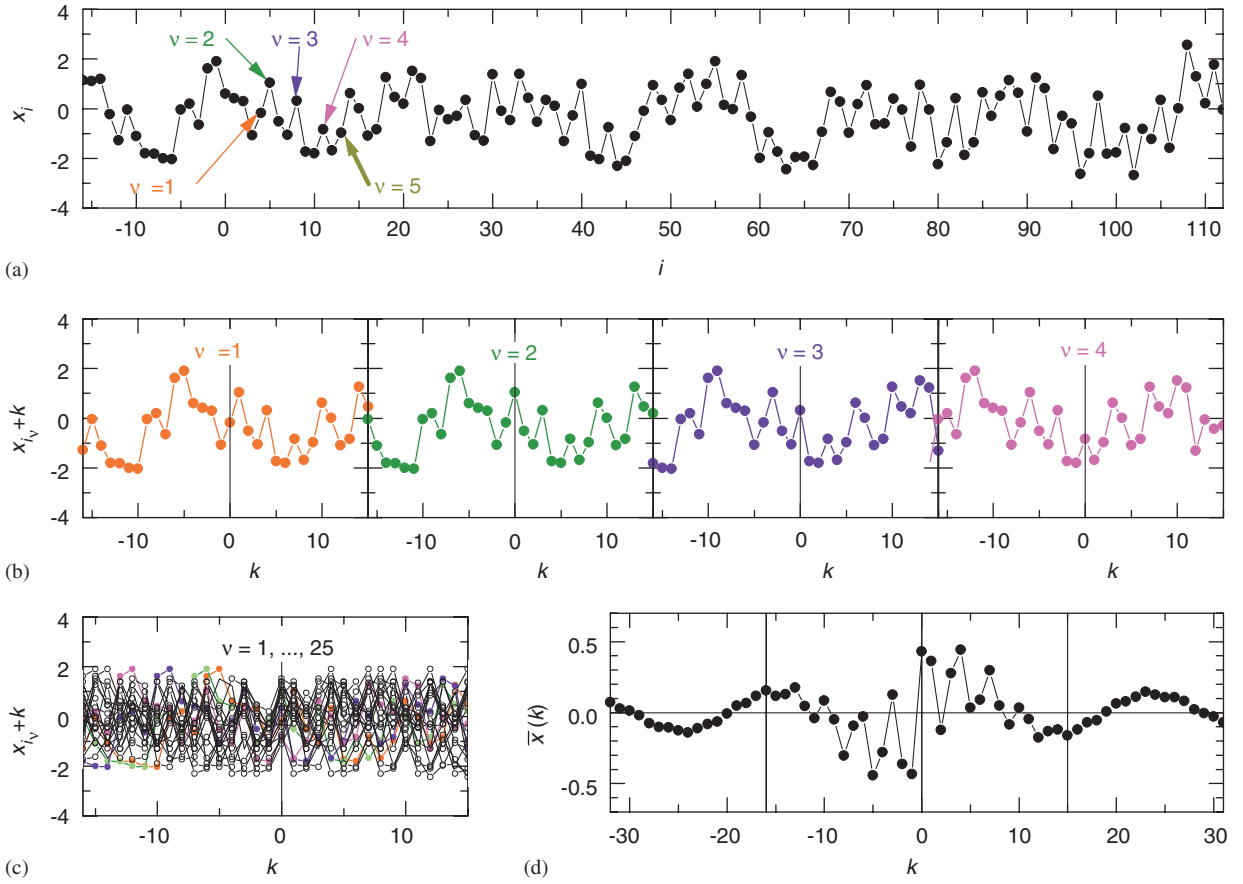

Fig. 1. Illustration of the PRSA technique: (a) Anchor points are selected from the original time series (x_i); here increase events are selected according to Eq. (1a), corresponding to $T = 1$. (b) Windows (surroundings) of length $2L$ with $L = 16$ are defined around each anchor point; the points in each window are given by Eq. (3) and shown here for the first four anchor points. (c) The surroundings of many anchor points (all located in the centre) are shown on top of each other. (d) The PRSA curve $\bar{x}(k)$ resulting from averaging over all surroundings is shown versus the offset k from the anchor points; the parameter L is increased to $L = 32$ in order to improve the visibility of the slow period. The original signal consists of $1/f$ noise (generated using the Fourier filtering method, see, e.g., Ref. [5]) with two additional quasi-periodicities with characteristic frequencies $f = 0.05/\Delta t$ and $f = 0.3/\Delta t$; phase jumps are inserted after an average number of four periods.

Note that typically half of all points of the time series will be anchor points by any of these definitions. The parameter T in Eq. (2) sets an upper frequency limit for the periodicities that can be detected by PRSA (low-pass filter). For $T = 1$, Eq. (2) is identical with the criteria (1), and no filter is applied. It can be shown mathematically[2] that the PRSA is most sensitive for strictly periodic oscillations with frequency $f \approx 1/(2.7\,T)$. This value changes to $f \approx 1/(2.5\,T)$ if the signal contains many phase jumps (non-stationarities). Additional criteria for the anchor points might be implemented in order to avoid that artefacts are selected as anchor points. For example, when considering heartbeat time series, extraordinary large increases might be excluded from causing anchor points since they are probably artefacts.

[2]In order to calculate the parameter T for which the PRSA can most effectively detect sinusoidal signals with frequency f, we consider—instead of the sums in Eq. (2)—the following integral:

$$\frac{1}{T}\int_0^T \sin(2\pi f x)\,\mathrm{d}x = \frac{1-\cos(2\pi f T)}{2\pi f T}.$$

Finding the maximum of this expression yields $T \approx 2.33/(2\pi f) \approx 1/(2.7f)$.

Quasi-periodic sinusoidal oscillations in the noisy series (x_i) will cause anchor points predominantly in the phase of the steepest ascent or decent, i.e., when the phase of the oscillation is close to 0 or π for the definitions (1a) and (1b), respectively. This way the phase information of the oscillations is obtained from the signal itself and the signal can be *phase-rectified* using the anchor points. Differences between the PRSA curves obtained with Eqs. (1a) and (1b) will indicate missing time-reversal symmetry of the original signal, and they allow to study separately processes occurring during increasing and decreasing parts.

In the *second step* (see Fig. 1(b)) of the PRSA method windows (surroundings) of length $2L$ are defined around each anchor point. Anchor points close to the beginning or the end of the time series, where no full surroundings of length $2L$ are available, are disregarded. If we denote the positions (indices) of all regarded anchor points by (i_v), $v = 1, \ldots, M$, the points in window number v, corresponding to anchor point i_v, will be

$$x_{i_v-L}, x_{i_v-L+1}, \ldots, x_{i_v}, \ldots, x_{i_v+L-2}, x_{i_v+L-1}. \tag{3}$$

Note that many of these windows will overlap, since many anchor points are close to each other. The parameter L should exceed the expected coherence time of the periodicities in the data; it must definitely be larger than the period of the slowest oscillation that one wants to detect.

In the *third step* (see Fig. 1(c) and (d)) the PRSA $\bar{x}(k)$ is obtained by averaging over all windows,

$$\bar{x}(k) = \frac{1}{M}\sum_{v=1}^{M} x_{i_v+k} \quad \text{for } k = -L, -L+1, \ldots, 0, \ldots, L-2, L-1. \tag{4}$$

In this average, non-periodic components that are not phase synchronized with the anchor points, i.e., non-stationarities, artefacts, and noise, cancel out, and only events that have a fixed phase relationship with the anchor points, i.e., all periodicities and quasi-periodicities, 'survive' the procedure. This uncovering of all periodicities and quasi-periodicities is illustrated in Fig. 1, where $1/f$ noise with two additional quasi-periodicities is analysed. One can clearly identify these periodicities in the phase-rectified average shown in Fig. 1(d). In addition, the coherence time of the fast quasi-periodicity can be estimated, which corresponds to the time for the decay of the fast oscillation, i.e., about four periods. The finite coherence time is a direct consequence of the non-stationary nature of the periodicity, where phase jumps were introduced each four periods. In order to observe the coherence time for the slower periodicity, the window size L would have to be increased further.

The performance of the PRSA technique on real biological data is shown in Fig. 2(a) and (c), where a (non-stationary and noisy) 24 h long-term recording of heartbeat intervals is shown together with the corresponding PRSA transformation. In the transformed data, Fig. 2(c), two relevant periodicities can be observed by eye. Note that the PRSA allows an assessment of the periodic content of long-term records by looking at a rather short 'distilled' signal, where all important periodic or quasi-periodic components of the original signal are centred around the middle ($k = 0$).

3. Comparison of PRSA with conventional spectral analysis and correlation analysis

Fig. 2 compares the frequency content of the original signal with that of the phase-rectified average. There are several similarities but also important distinctions between the power spectrum of the phase-rectified average, $P_{\mathrm{PRSA}}(f)$, and the conventional power spectrum $P(f)$. Both power spectra show peaks for the characteristic periodic components of the signal, but the peaks appear much clearer in the phase-rectified spectrum (Fig. 2(d)) than in the conventional power spectrum (Fig. 2(b)). This improved signal-to-noise ratio is *not* primarily due to the broader binning of the PRSA data, but can be substantiated by two main arguments as follows.

The first argument for the advantage of the PRSA over conventional spectral analysis is based on the way the signal is compared with continuous, uninterrupted sinusoids in spectral analysis. If the signal consists of many short patches of periodicities with a particular frequency, some of the patches will be in phase with the analysing sinusoid, while most will rather be out of phase, i.e., show phase shifts between 0 and 2π. The number of patches in phase with the analysing sinusoid will approximately equal the number of patches with

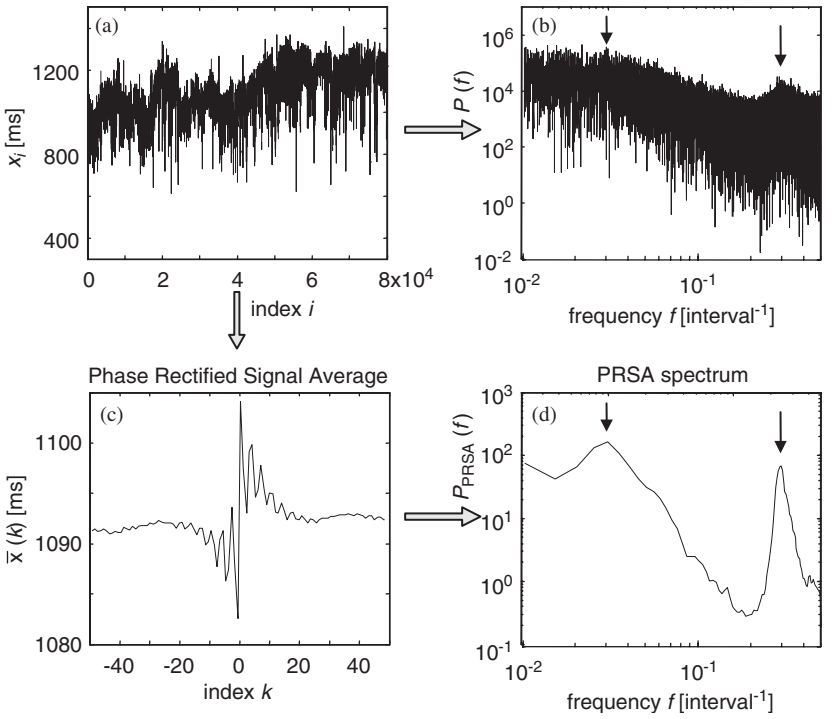

Fig. 2. Comparison of (a) the original signal x_i (series of beat-to-beat intervals recorded over 24 h in a post-infarction patient), (b) the corresponding power spectrum of the original data, (c) the PRSA transform $\bar{x}(k)$ calculated with $T = 1$ and $L = 50$ using anchor point condition Eq. (1a), (d) the power spectrum of the PRSA transform. Two frequency peaks corresponding to quasi-periodicities are indicated by arrows; they can be recognized much more clearly in the PRSA spectrum.

phase shifts of π. These two types of patches have contributions with opposite sign to the corresponding Fourier coefficient, and hence their contributions will approximately cancel. The same is true for all patches with phase shifts differing by π. Only the small number of patches that happen to have no corresponding patch with phase shift differing by approximately π will give an observable contribution to the Fourier coefficient and affect the power spectrum. This is the reason for the noisy structure of conventional power spectra as the one shown in Fig. 2(b).

In the PRSA, on the other hand, the anchor points are determined from the signal itself. Hence, the anchor points are always phase synchronized with the signal, even if the phase is unstable or non-stationarities occur. Since all patches are aligned with respect to their phase of oscillation (i.e., phase-rectified), the synchronization of the signal patches is ensured, and all patches can contribute to the PRSA signal and its power spectrum.

The second argument in favour of the PRSA is based on the different scaling behaviour of the corresponding power spectra. To show this difference we consider the probability p_f that a specific oscillating component with frequency f, $x_f(t) = A_f \sin(2\pi ft)$, occurring in $x(t) = x_{t/\Delta t}$ affects the PRSA $\bar{x}(t)$. Because of the linear averaging procedure in Eq. (4) the effect of $x_f(t)$ is proportional to its amplitude factor A_f, and therefore $p_f \sim A_f$. In addition, $x_f(t)$ has to cause anchor points t_v, since positive and negative parts of $\sin(2\pi ft)$ otherwise cancel in the averaging procedure. Thus, for the anchor point criterium in Eq. (1a), $x_f(t_v)$ must be larger than $x_f(t_v - \Delta t) \approx x_f(t_v) - \Delta t x'_f(t_v) = x_f(t_v) - \Delta t 2\pi f A_f \cos(2\pi ft_v)$, which is a valid approximation with the exception of very high frequencies f. The maxima of $x_f(t_v) - x_f(t_v - \Delta t) = 2\pi\Delta t f A_f \cos(2\pi ft_v)$ occur for $t_v = n/f$ with any integer n. Since anchor points t_v are generated primarily at or close to phase zero of the considered component, the averaging procedure is phase-rectifying. The value of the maxima of $x_f(t_v) - x_f(t_v - \Delta t)$ is $2\pi\Delta t f A_f$. Hence, the probability to anchor the averaging procedure is proportional to $A_f f$ ($2\pi\Delta t$ are unimportant pre-factors); i.e., we get in total $p_f \sim A_f^2 f$. In $\bar{x}(t)$ the amplitude of the considered spectral component with frequency f is thus determined by $A_f^2 f$ instead of A_f.

This has direct consequences for the power spectrum, because it is always proportional to the square of the amplitude. If we consider $1/f^{\beta}$ noise, where

$$P(f)\sim A_f^2\sim f^{-\beta} \tag{5}$$

we obtain

$$P_{\mathrm{PRSA}}(f)\sim p_f^2\sim A_f^4 f^2\sim f^{-2\beta+2}=f^{-\beta'} \quad \text{with } \beta'=2\beta-2. \tag{6}$$

This relation is generally valid for all values of the spectral exponent β. In the special case of $1/f$ noise ($\beta=1$), which is particularly prevalent in biological and other natural signals, the PRSA spectrum is flat, $\beta'=0$. This has consequences for the detection of deviations from the standard scaling behaviour that are caused by quasi-periodicities. They can be identified significantly easier when studying the nearly constant $P_{\mathrm{PRSA}}(f)$ instead of $P(f)$.

There is ample evidence that many natural records exhibit long-term correlations. Prominent examples include turbulence data, economic volatility records, meteorological, hydrological, and climatological data, as well as heartbeat and breathing records and DNA sequences (for references, see, e.g., Refs. [6–8]). Long-term correlations are characterized by a power-law decay of the autocorrelation function of the normalized data $\xi_i=(x_i-\langle x_i\rangle)/(\langle x_i^2\rangle-\langle x_i\rangle^2)^{1/2}$, $i=1,\ldots,N$,

$$C(s)=\frac{1}{N-s}\sum_{i=1}^{N-s}\xi_i\xi_{i+s}\sim s^{-\gamma}, \tag{7}$$

where the correlation exponent γ is related to β from Eq. (5) by $\beta=1-\gamma$ if $0\leqslant\beta<1$. For non-stationary data, improved techniques for the detection of long-term correlations and the determination of the scaling exponents have been established. For example in the detrended fluctuation analysis (DFA) method one determines the scaling behaviour of the detrended fluctuation function $F(s)\sim s^{\alpha}$, where the scale s is similar to the s in Eq. (7) and the fluctuation exponent α is related to β by $\alpha=(\beta+1)/2$ if $\beta>0$ [9,10].

Fig. 3 shows the PRSA signals and their power spectra for long-term correlated data with different scaling exponents β. While the PRSA signals in Fig. 3(a) turn out to be rather featureless, the power spectra in Fig. 3(b) confirm the scaling behaviour predicted in Eq. (6). We conclude that in studying purely long-term correlated data, the PRSA has no important advantages over conventional spectral analysis and should also not replace the DFA method. However, any deviations from such ideal scaling behaviour will be shown very clearly by the PRSA, since the long-term correlations in the background do not disturb the picture.

4. Quantitative characterization of the PRSA curve

As shown in the previous section the power spectrum of the PRSA curve has some advantages over the conventional power spectrum, especially if additional quasi-periodicities have to be identified in $1/f$ noise. However, it is still not really appropriate to compare the compressed signal $\bar{x}(k)$ with sinusoids that comprise the whole window width from $k=-L$ to $L-1$ with identical amplitude. In $\bar{x}(k)$ all periodicities are aligned in the centre, i.e., for $k=0$, and decay towards larger positive or negative k if the coherence time is finite (see, e.g., Fig. 1(d)). This has two important consequences: (i) the central peak of the PRSA curve contains contributions of all (quasi-) periodicities in the original signal and (ii) the decay of the oscillations towards large $|k|$ conveys information about their coherence time. In addition, an asymmetry of the PRSA curve will indicate a break of time-reversal symmetry, which cannot be seen in any power spectra. Hence, in some applications it can be useful to characterize $\bar{x}(k)$ by certain values or slopes at specific distances from the centre. Such parameters, however, will have to be selected according to specific problems, and no general characterization of $\bar{x}(k)$ or all quasi-periodicities in the original data can be expected from them.

To avoid the shortcomings of the power spectra and obtain frequency-specific as well as time-specific information, we suggest to employ wavelet analysis for the study of $\bar{x}(k)$ since it allows to select both the time scale (inverse frequency) and the time position relative to the centre. This way, the frequencies and the coherence times in both time directions can be studied for all quasi-periodicities.

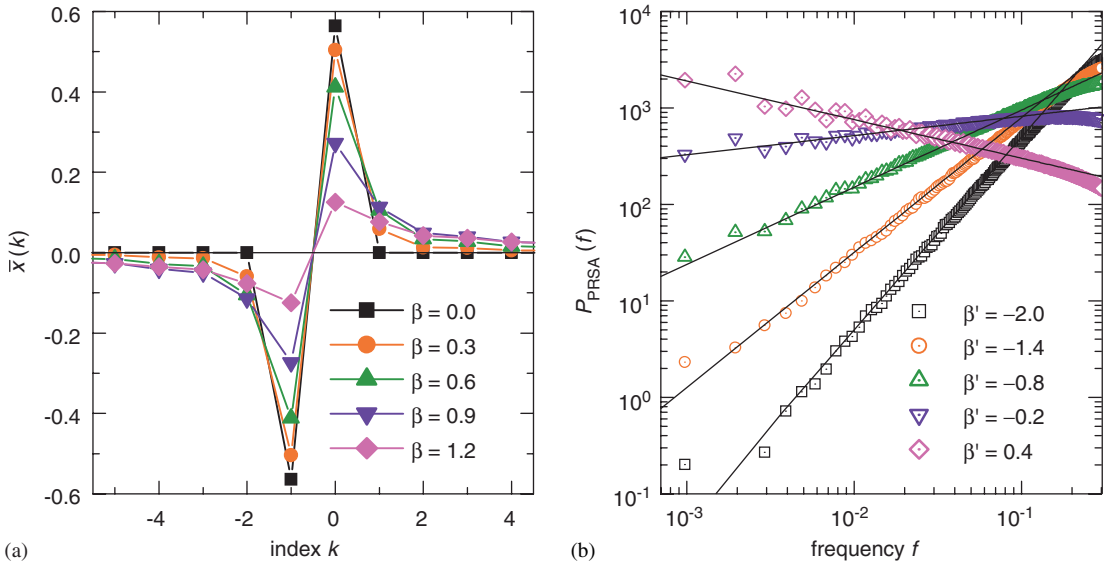

Fig. 3. PRSA study of $1/f^{\beta}$ noise with spectral scaling exponents $\beta = 0.0$ (□), 0.3 (○), 0.6 (△), 0.9 (▽), and 1.2 (◇); i.e., long-term correlated data. (a) The PRSAs $\bar{x}(k)$ calculated with $T = 1$ and $L = 5$ using anchor point condition, Eq. (1a), show only a central oscillation with a width and height that depend on β. (b) The corresponding power spectra exhibit scaling behaviour $P_{\mathrm{PRSA}}(f) \sim f^{-\beta'}$ with $\beta' = 2\beta - 2$ confirming Eq. (6). The data have been generated using the Fourier filtering method, see, e.g., Ref. [5].

The (continuous) wavelet transform of a signal $\bar{x}(t)$ is defined as [12–15]

$$\tilde{x}_w(s,p) = \int_{-\infty}^{+\infty} \bar{x}(t) w[(t-p)/s] \mathrm{d}t \tag{8}$$

with the two variables scale s and position p. Here, $w(t)$ is the mother wavelet, a localized function. Examples for continuous common wavelets include derivatives of Gaussians like

$$g_1(t) = t \exp(-t^2/2), \tag{9}$$

(first derivative) and $g_2(t) = (t^2 - 1)\exp(-t^2/2)$ (second derivative, 'Mexican Hat' wavelet). Another popular wavelet is the Haar wavelet,

$$h(t) = -1 \text{ (for } -1 \leqslant t < 0), \ +1 \text{ (for } 0 \leqslant t < 1), \ 0 \text{ (else)}. \tag{10}$$

The discretized version of the wavelet transform, Eq. (8), which shall be applied to the PRSA signal $\bar{x}(k)$ reads $\tilde{x}_w(s,p) = \sum_{k=-L}^{L-1} \bar{x}(k) w[(k-p)/s]$.

Fig. 4 shows a greyscale plot of the squares of these wavelet coefficients $\tilde{x}^2_{g_1}(s,p)$ for wavelet $g_1(t)$ from Eq. (9) versus time scale s and time position p for signals similar to those considered in Fig. 1, i.e., $1/f$ noise with two quasi-periodicities, but with different coherence times of the oscillations. The characteristic frequencies of the two quasi-periodicities can be clearly seen by looking along the scale axis, while their coherence time scales can be seen by looking along the time shift (position) axis. The parts (a–c) correspond to different average coherence times of four, two and one period. Since squares of the wavelet coefficients are considered, two stripes to the left and to the right of the $p = 0$ line correspond to a coherence time of one oscillation period. The wavelet transform of the PRSA for $1/f$ noise without additional periodicities (similar to the curves in Fig. 3(a)) is shown in Fig. 4(d) for comparison.

A comparison of the squared central wavelet amplitudes $\tilde{x}^2_{g_1}(s,0)$ for the same data as in Fig. 4(a–d) is plotted in Fig. 5 versus (time) scale s. For the data with the two additional quasi-periodicities, one can clearly observe the two corresponding peaks; the curves are quite independent of the coherence times. However, the quantitative time scale s of the peaks depends on the chosen wavelet, and it has to be multiplied by a wavelet-

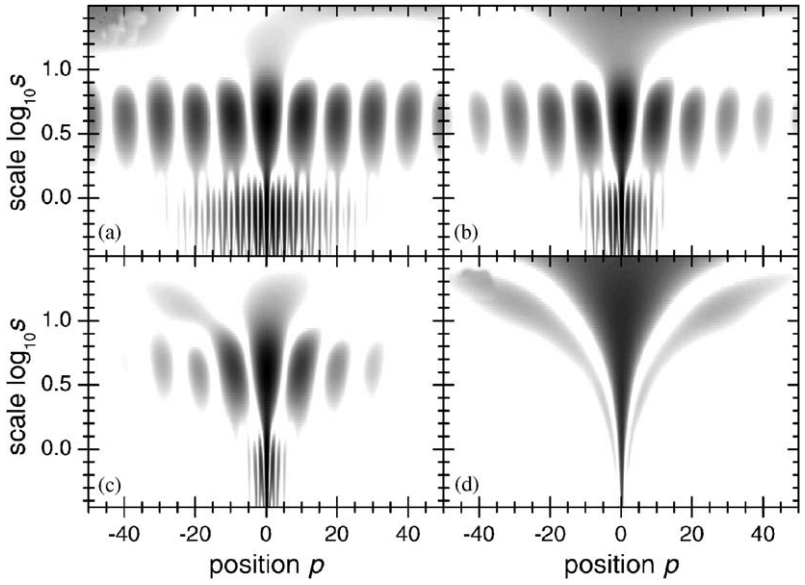

Fig. 4. Grey scale plots of the squared PRSA wavelet coefficients $\tilde{x}^2_{g_1}(s,p)$ for $1/f$ noise with two additional quasi-periodicities of frequencies $f = 0.05/\Delta t$ and $f = 0.3/\Delta t$ (a–c) and pure $1/f$ noise (d). Phase jumps are inserted after an average number of (a) four, (b) two, and (c) one period(s). The wavelet coefficients were calculated based on $\bar{x}(k)$ with $T = 1$ and $L = 100$ using anchor point condition Eq. (1a) and wavelet transform with the wavelet according to Eq. (9). The logarithmic grey scale ranges from $\tilde{x}^2_{g_1}(s,p) < 0.005$ (white) to > 0.25 (black). The results for 10^3 time series of length $N = 2^{15}$ were averaged for each plot.

specific factor to obtain the inverse frequency of the periodicity. For example, for $g_1(t)$ (Eq. (9)) a scale s corresponds to the frequency $f \approx 0.22/(s\Delta t)$. The central wavelet amplitude thus carries the information about the time scales (frequencies) of the periodicities in the data, while the non-central wavelet amplitudes carry the information about their coherence times.

Fig. 5 also shows two curves that were obtained for modulated quasi-periodicities illustrating that anchor points based on increases and decreases allow to distinguish processes occurring during increasing and decreasing parts of the signal. Here, the high-frequency oscillation is modulated by the low-frequency oscillation such that it only occurs if the low-frequency oscillation is in its increasing phase. The resulting PRSA curves for the anchor point criteria (1a) and (1b) are shown in the inset. One can see that the two curves are only approximately symmetric. In the other signals studied in this paper, both anchor point criteria led to fully symmetric PRSA curves. Now the amplitude of the curve for anchor points based on increases (circles) is slightly larger than the amplitude of the curve for anchor points based on decreases (triangles). This can be seen more clearly in the main part of the figure where the squared central wavelet amplitudes $\tilde{x}^2_{g_1}(s,0)$ are shown also for the modulated data. Hence, the difference of PRSA curves (and the corresponding central wavelet amplitudes) for Eqs. (1a) and (1b) allow to study separately processes occurring during increasing and decreasing parts of the signal.

Fig. 6(a) shows the effect of two synchronized periodicities on the squared wavelet amplitudes $\tilde{x}^2_{g_1}(s,p)$ of the PRSA transform. One can see that pronounced connections between the frequency peaks corresponding to the two components occur. For Fig. 6(b) the amplitudes of both periodicities are increasing within each coherent oscillation patch, which leads to a signal with a non-stationary and non-time-reversal symmetric amplitude. More coherent periods can be observed in the future (to the right of the anchor points at $p = 0$) than in the past (to the left). Hence, the PRSA transform can reveal non-stationarities in the amplitude of the analysed periodicities, i.e., properties definitely not available in studies of power spectra.

Similar results as for the continuous wavelets can be obtained for the Haar wavelet, Eq. (10), see Fig. 6(c,d). Note, however, that the sharp drop of $h(t)$ at $t = \pm 1$ causes some curved artefact structures in Fig. 6(c), which

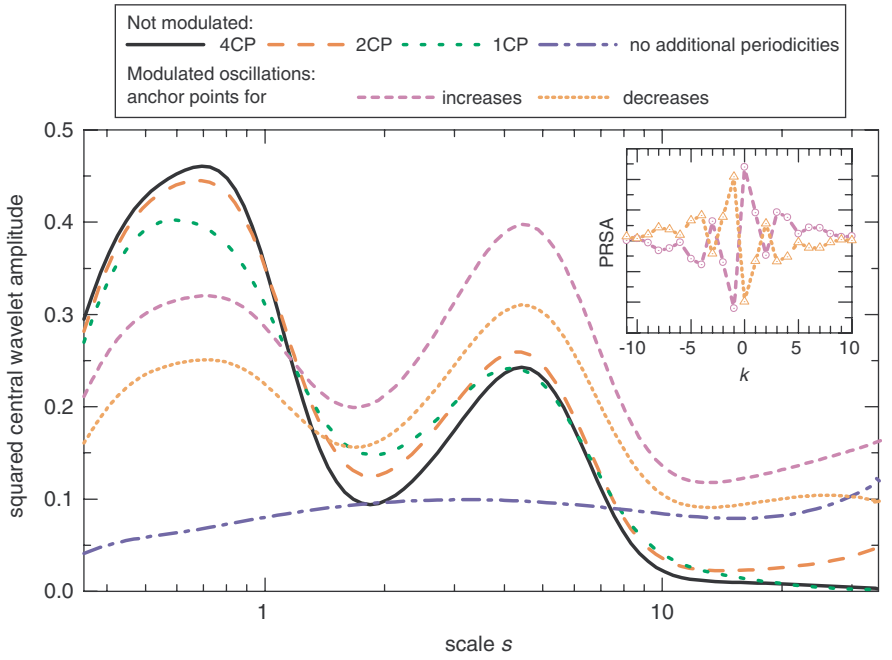

Fig. 5. The squared central wavelet amplitude $\tilde{x}^2_{g_1}(s,0)$ plotted versus (time) scale s for the same data as in Fig. 4(a–d), $1/f$ noise with two quasi-periodicities at $f = 0.05/\Delta t$ and $0.3/\Delta t$ and coherence times of four (solid line), two (dashed line), and one (dotted line) period(s) (CP = coherence periods). The dash-dotted line is for the pure $1/f$ noise, where all peaks are clearly absent. The short-dashed line and short-dotted line correspond to data with modulated periodicities where the high-frequency oscillation is modulated by the low-frequency oscillation such that it only occurs if the low-frequency oscillation is in its increasing phase. The corresponding PRSA curves are shown in the inset. The curves are based on the PRSA with anchor points according to definitions (1a) (short-dashed line, circles) and (1b) (short-dotted line, triangles).

might disturb the determination of the coherence time scale for the slower periodicity. However, for the central wavelet amplitude, results based on $h(t)$ are equivalent with those based on $g_1(t)$.

5. Test with surrogate heartbeat data and possible applications

In order to test the capability of the PRSA method for the detection of quasi-periodicities in realistic data, we have simulated long-term surrogate heartbeat records ($N \approx 95,000$ heartbeats, corresponding to 24 h ECGs) using the model described in Ref. [16]. The model generates non-stationary data with transient correlations, i.e., correlations of different strength and different typical duration within finite segments of the signal. The exponents and crossovers characterizing the correlations and quasi-periodicities (e.g., breathing sinus arrythmia) in the signal and in its variance are tuned to generate model time series which are in agreement with data of heartbeat dynamics observed during wake and during different sleep stages. To test the PRSA method, we have added a piecewise periodic component $x_{f_0}(t) = A\sin(2\pi f_0 t)$ with phase shifts after each 4th period on average. The frequency was set to $f_0 = 0.1$ inverse heartbeats (Δt^{-1}), which is of the order of the frequencies occurring in Mayer waves (not simulated in the considered model). The amplitude of the periodic component was systematically varied.

Fig. 7 shows the average PRSA central wavelet amplitudes $\tilde{x}_{g_1}(2.2,0)$ and $\tilde{x}_h(2.2,0)$ and the total power in the band $0.095 < f < 0.105$ inverse heartbeats (calculated by Fourier transform of the original signal) versus the amplitude A. For very low amplitudes, $A < 10^{-2}$, all quantities are approximately constant, showing that such weak additional periodicities cannot be detected. Note, that the error bars, which characterize the fluctuations for 100 simulated records, are quite narrow for the PRSA central wavelet amplitudes (see magnification in the inset) but fairly large for the total power in the spectral narrow band. If the error bars are taken into account,

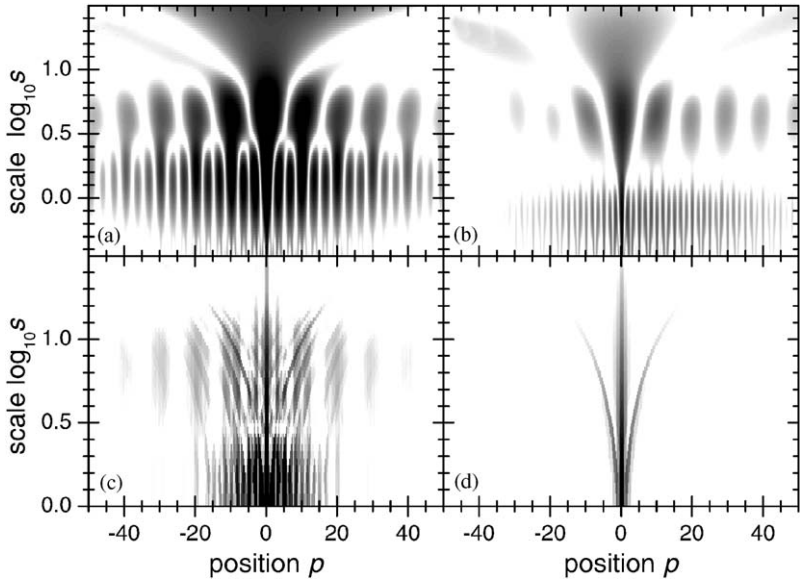

Fig. 6. Grey scale plots of the squared PRSA wavelet coefficients for $1/f$ noise with two additional quasi-periodicities like in Fig. 4. (a) The two periodicities ($f = 0.05/\Delta t$ and $0.15/\Delta t$) are phase synchronized which leads to pronounced lines connecting the corresponding peaks. (b) The amplitudes of both periodicities ($f = 0.05/\Delta t$ and $0.3/\Delta t$) are increasing from 0.05 to 2 within each stationary patch. Hence, the time-reversal symmetry is broken, and more coherent periods can be observed in the future (to the right of the anchor points at $p = 0$) than in the past (to the left). (c,d) The same as Fig. 4(b,d) but for a wavelet transform with Haar wavelets according to Eq. (10). Here, the logarithmic grey scale ranges from $\tilde{x}_h^2(s,p) < 0.001$ (white) to > 0.1 (black).

the thresholds for the reliable detection of the additional quasi-periodicity are $A_{\min} = 1.9 \times 10^{-2}$, 2.1×10^{-2}, and 8.0×10^{-2} for the two wavelet coefficients and for conventional spectral analysis, respectively. Hence, the PRSA-based central wavelet amplitudes are clearly superior, since the corresponding thresholds are about 75% lower.

The detection of quasi-periodicities in long-term records of human heart rate is of high clinical relevance. Quasi-periodicities reflect regulation processes of the autonomic cardiac nervous system. Autonomic dysfunction is closely related to cardiac mortality and susceptibility to life-threatening arrhythmic events [17]. Consequently, assessment of heart rate variability based on spectral analysis has been proposed for risk prediction [18]. However, no established parameter with sufficiently high prognostic value has been identified yet [11]. As shown in Fig. 2 and by the simulation results presented in Fig. 7, PRSA yields significant advantages over conventional methods in detection of quasi-periodicities in long-term records of human heart rate. Moreover, PRSA offers the possibility to selectively analyse acceleration- and deceleration-related periodic behaviour in human heart rate which might provide more differentiated insights into cardiac autonomic regulation processes.

Further possible applications of PRSA in biology and physiology include rhythmic motions of limbs in walking, muscle contractions, rhythms underlying the release of hormones that regulate growth and metabolism, periodicities in gene expression, membrane potential oscillations, oscillations in neuronal signals, and circadian rhythms [1,2]. We believe that the range of suitable applications for the PRSA method also includes quasi-periodic geophysical data, e.g., the El-Nino phenomenon, sunspot numbers, and ice age periods [3]. In addition, the analysis of complex elastic wave patterns to study seismic events or to determine material properties of granular matter might be improved by PRSA. The study of non-stationary quasi-periodic complex waveforms is also a common task in the analysis and recognition of speech or music.

Besides the PRSA technique for single time series, a modification of the method that allows the study of cross-correlations between two non-stationary signals seems promising. Our work on such a cross-correlation PRSA technique where the anchor points are derived from one signal while the averaging is performed with another signal is in progress.

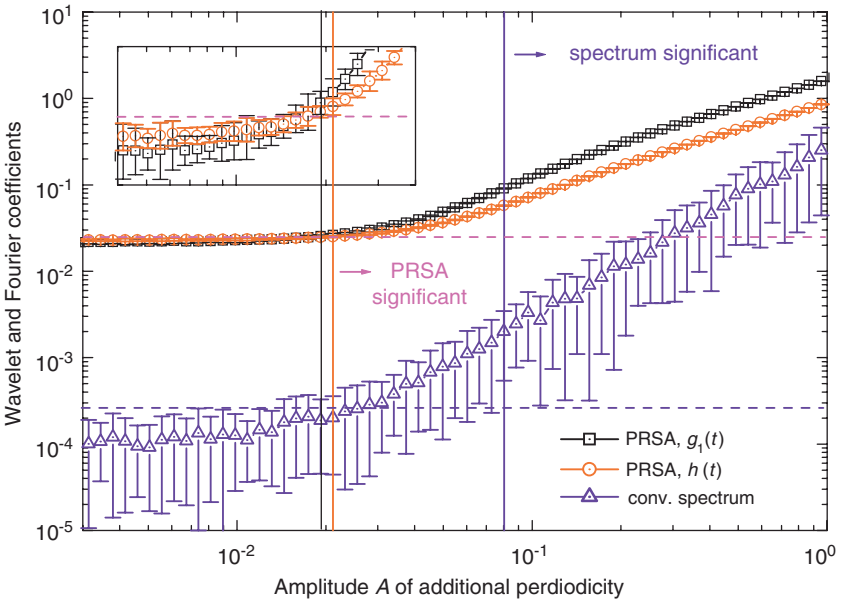

Fig. 7. PRSA central wavelet amplitudes $\tilde{x}_{g_1}(2.2,0)$ (squares) and $\tilde{x}_h(2.2,0)$ (circles), and total power in the band $0.095<f<0.105$ inverse heartbeats (triangles, calculated by Fourier transform of the original signal) versus the amplitude A of the additional (sinusoidal) quasi-periodicity of frequency $f_0 = 0.1$ inverse heartbeats. The underlying non-stationary surrogate heartbeat data have been generated using a model for data with transient correlations, i.e., correlations of different strengths and different typical durations within finite segments of the signal [16]. The error bars show the fluctuations occurring in the 100 configurations we considered; note that the error bars are asymmetric due to the logarithmic plot. The detection thresholds (vertical lines) have been determined using the horizontal dashed lines, which mark the limit values for the coefficients: for small A, all mean coefficients and error bars are below the dashed lines (for the central wavelet amplitudes, see enlarged part in the upper left corner), and above the detection thresholds all mean coefficients and error bars remain above the dashed lines.

Acknowledgements

We thank K. Hnatkova, H. Huikuri, T. Mäkikallio, A. Schömig, and K. Ulm for discussions. This study was supported by grants from the Bundesministerium für Bildung, Wissenschaft, Forschung und Technologie (No. 13N7073/7), from the Kommission für Klinische Forschung, and from the Deutsche Forschungsgemeinschaft (SFB 368 and Grant KA 1676/3).

References

[1] J.J. Tyson, Biochemical oscillations, in: C. Fall, E. Marland, J. Wagner, J. Tyson (Eds.), Computational Cell Biology: An Introductory Text on Computer Modeling in Molecular and Cell Biology, Springer, New York, 2002.
[2] L. Glass, Nature 410 (2001) 277.
[3] H. von Storch, F.W. Zwiers, Statistical Analysis in Climate Research, Cambridge University Press, Cambridge, 2001.
[4] M. Ahdesmäki, H. Lähdesmäki, R. Pearson, H. Huttunen, O. Yli-Harja, BMC Bioinformatics 6 (2005) 117.
[5] H.A. Makse, S. Havlin, M. Schwartz, H.E. Stanley, Phys. Rev. E 53 (1996) 5445.
[6] S. Havlin, S.V. Buldyrev, A. Bunde, A.L. Goldberger, P.Ch. Ivanov, C.-K. Peng, H.E. Stanley, Physica A 273 (1999) 46.
[7] A. Bunde, J.W. Kantelhardt, Phys. Bl. 57 (2001) 49.
[8] A. Bunde, J. Kropp, H.-J. Schellnhuber (Eds.), The Science of Disasters—Climate Disruptions, Heart Attacks, and Market Crashes, Springer, Berlin, 2002.
[9] C.-K. Peng, S.V. Buldyrev, S. Havlin, M. Simons, H.E. Stanley, A.L. Goldberger, Phys. Rev. E 49 (1994) 1685.
[10] J.W. Kantelhardt, E. Koscielny-Bunde, H.H.A. Rego, S. Havlin, A. Bunde, Physica A 295 (2001) 441.
[11] Task Force of the European Society of Cardiology and the American Society of Pacing and Electrophysiology, Circulation 93 (1996) 1043.
[12] P. Goupillaud, A. Grossmann, J. Morlet, Geoexploration 23 (1984) 85.
[13] I. Daubechies, Commun. Pure Appl. Math. 41 (1988) 909.

[14] S. Mallat, IEEE Trans. Pattern Anal. Machine Intell. 11 (1989) 674.
[15] P. Addison, Phys. World 17 (2004) 35.
[16] J.W. Kantelhardt, S. Havlin, P.Ch. Ivanov, Europhys. Lett. 62 (2003) 147.
[17] B. Lown, R.L. Verrier, New Engl. J. Med. 294 (1976) 1165.
[18] J. Bigger Jr., J.L. Fleiss, R.C. Steinman, L.M. Rolnitzky, R.E. Kleiger, J.N. Rottman, Circulation 85 (1992) 164.